

# Asymmetrical estimator for training grey-box deep photonic neural networks

Yizhi Wang<sup>1</sup>, Minjia Chen<sup>1</sup>, Chunhui Yao<sup>1</sup>, Jie Ma<sup>2</sup>, Ting Yan<sup>2</sup>, Richard Penty<sup>1</sup>, Qixiang Cheng<sup>1,2\*</sup>

<sup>1</sup> Centre for Photonic Systems, Electrical Engineering Division, Department of Engineering, University of Cambridge, Cambridge, CB3 0FA, UK

<sup>2</sup> GlitterinTech Limited, Xuzhou, China

\* Corresponding: qc223@cam.ac.uk

## Abstract

Physical neural networks (PNNs) are emerging paradigms for neural network acceleration due to their high-bandwidth, in-propagation analogue processing. Despite the advantages of PNN for inference, training remains a challenge. The imperfect information of the physical transformation means the failure of conventional gradient-based updates from backpropagation (BP). Here, we present the asymmetrical training (AT) method, which treats the PNN structure as a grey box. AT performs training while only knowing the last layer output and neuron topological connectivity of a deep neural network structure, not requiring information about the physical control-transformation mapping. We experimentally demonstrated the AT method on deep grey-box PNNs implemented by uncalibrated photonic integrated circuits (PICs), improving the classification accuracy of Iris flower and modified MNIST hand-written digits from random guessing to near theoretical maximum. We also showcased the consistently enhanced performance of AT over BP for different datasets, including MNIST, fashion-MNIST, and Kuzushiji-MNIST. The AT method demonstrated successful training with minimal hardware overhead and reduced computational overhead, serving as a robust light-weight training alternative to fully explore the advantages of physical computation.

## Introduction

Neural network (NN)-based machine learning algorithms are prevalently used in the state-of-the-art industry and academia research<sup>1-3</sup>. Physical neural networks (PNNs) are emerging schemes for NN acceleration, whose capability is not limited to the increased parallelism seen in many dedicated digital hardware such as GPU<sup>4</sup> or TPU<sup>5</sup>, but also capable of achieving high-bandwidth and in-propagation analogue computation<sup>6,7</sup>.

Nevertheless, their implementation is known to be challenging<sup>8,9</sup>. One persisting difficulty is the lack of suitable training methods. Despite the gradient-based optimizer with backpropagation<sup>10</sup> (BP) is an industry standard for training digital NNs, BP's inability to deal with inaccurate network information results in sizeable degradation of the network performance<sup>11</sup>. Therefore, it is desirable to find alternatives which enjoy the advantages of BP (robustness, simple computation), while fully tailoring towards the characteristics of PNNs.

Whilst a common logic is to find an accurate mapping of the physical parameters for BP, the confinement of the PNN onto a describable mathematical model is antithetical to the motivation for physical computation. With physical computation, it is advantageous to embrace the complexity of the system and utilize those characteristics as useful resources. The uniqueness of physical computation, which is not replaceable by digital processing, can be seen in computing schemes such as reservoir computing<sup>12,13</sup> and Ising computing<sup>14,15</sup>. The retroaction of limiting the physical system's representation undermines the advantages of physical computations.

It is thus desirable to conduct network training not for the reconstructed mathematical representation of the physical system, but instead training the system as a grey box with a perturbate-able physical transformation. By grey-box training, we are limiting ourselves to only a minimal level of knowledge for the system, requiring only the input sample information, the topological connectivity of neurons, and the output prediction. All the details of the intermediate connections are not required and are hidden as a part of the grey box for the physical system. Here we present the asymmetrical training (AT) method for training a PNN structure as a grey box. The AT method serves as

an update direction estimator, replacing the BP gradient directions for conventional optimizers such as stochastic gradient descent (SGD)<sup>16,17</sup> and Adam<sup>18</sup>. It utilizes a parallel model for the concept of alignment<sup>19,20</sup> and allows the characteristics of the physical system to assist the training. The elimination of mapping the PNN as a mathematical description allows various advantages including training without the need for pre-training calibration, saving resources with reduced need to access information via readouts, and reduced cost via reducing both hardware and computational overheads.

In this paper, we demonstrate the power of the AT method with photonic integrated circuit (PIC) PNNs. Photonics is widely known for its high-bandwidth and multiplexing ability in multiple domains<sup>21-24</sup>. The matrix-vector multiplication accelerator with both on-chip<sup>25,26</sup> and free-space<sup>27,28</sup> optics already reveals great potential for photonic processing<sup>29,30</sup> in general. Especially, demonstrations of integrated photonic NNs have shown superior performance in both processing speed<sup>31</sup> and energy efficiency<sup>32</sup>. We start by describing the procedure and concept of the AT method, followed by the experimental demonstration of its capability to enhance performance with encapsulated systems for fast processing and variable-sized systems for general construction of PNNs. With completely calibration-free integrated photonic classifiers, the AT method still demonstrates its power to retrieve performance near the theoretical maximum for a grey box system, improving the accuracy from 38% (BP) to 97% (AT) for the Iris flower dataset, and from 29% (BP) to 84% (AT) for a modified MNIST hand-written digit dataset. Then, we apply the AT method for tasks of varying complexities (MNIST<sup>33</sup>, fashion-MNIST<sup>34</sup>, and Kuzushiji-MNIST<sup>35</sup>), showing its enhanced performance from BP across datasets. We finish by discussing the AT method’s advantages over other alternatives and its suitability for integrated PNN systems.

## Results

### Asymmetrical training method

The general mathematical description of a time-independent deep artificial neural network (DNN) is expressed in Eq. (1). The net output  $\mathbf{z}$  for a given layer  $[l]$  is determined by the connection strength of  $\mathbf{W}$  and bias  $\mathbf{b}$  acting on the activation level  $\mathbf{a}$  from the previous layer. The neuron’s activation level is modulated by some nonlinearity  $g(\cdot)$ .

$$\mathbf{z}^{[l]} = \mathbf{W}^{[l]}\mathbf{a}^{[l-1]} + \mathbf{b}^{[l]}; \mathbf{a}^{[l]} = g^{[l]}(\mathbf{z}^{[l]}) \quad (1)$$

For a PNN system, we focus on the neuron connectivity embodied by the topology of the system. With a static topology and some physical nonlinearity, we see the neuron activation level from the PNN as the result of some physical transformation which is perturbate-able by some physical controllable parameters. With the AT method, we eliminate the need to know the mapping relationship between the controls and physical transformation. The PNN is treated as an enclosed grey box, with access to only the sample input, topological neuron connectivity, and the output at the last layer of the deep structure. The inaccuracy of the input knowledge is also acceptable given it is a systematic deviation. (See Supplementary S1 for discussion on differences between implementing PNNs and utilizing physical devices for mathematical NNs.)

The AT method starts with the construction of a mathematical parallel model of the known connectivity same as the physical system. For the range of possible settings of the physical system, we hypothesize an estimated mapping profile between the controls and physical transformation. This deduced mapping serves as the reference for perturbing the PNN.

In the standard training of a DNN, we initialize the system with a random set of parameters. These parameters are then optimized for a quantifiable performance metric, which is typically the loss function  $L$  for measuring the separation between the prediction and the target. The updates for optimizers such as SGD and Adam are usually computed by BP, which is essentially auto-differentiation of the loss function with respect to the network parameters. We invoke a simple update expression for gradient descent under the regulation of learning rate  $\alpha$ .

$$\mathbf{W}^{[l]} = \mathbf{W}^{[l]} - \alpha\Delta\mathbf{W}^{[l]} \quad (2)$$

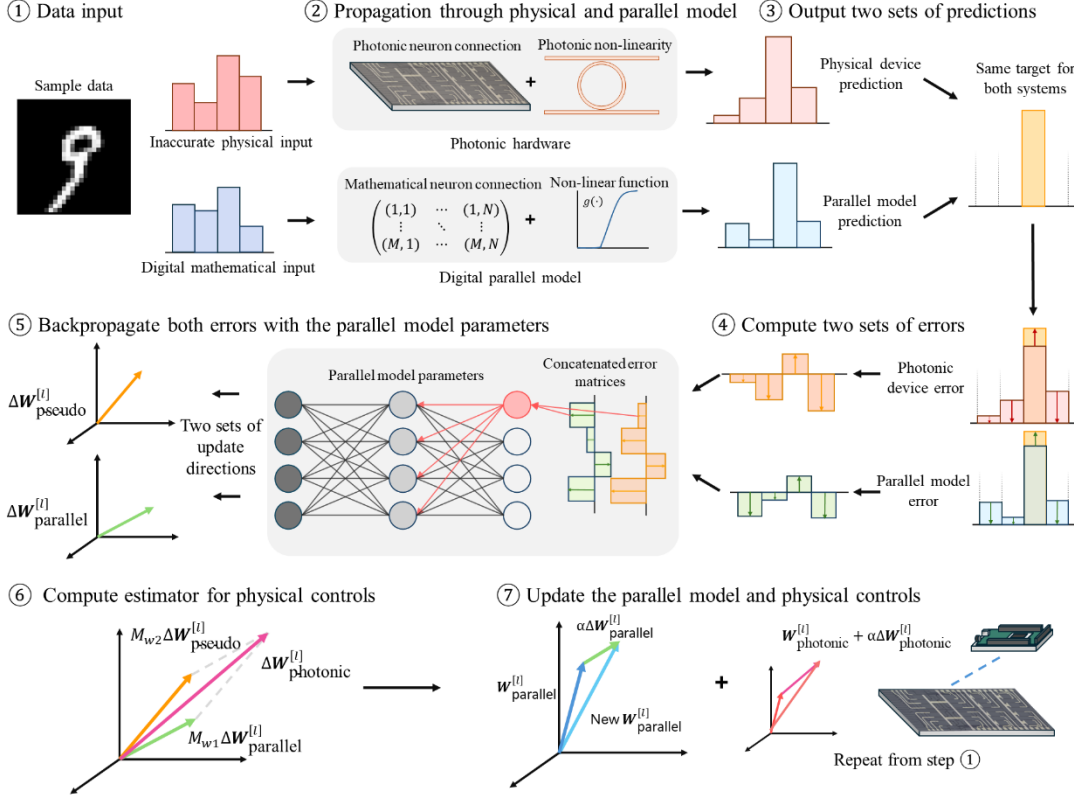


Fig.1 Workflow for the AT method to train a grey-box PNN. The training initializes with the construction of a physically relevant parallel model to be trained alongside the physical device. The tunable physical parameter controls are determined by an estimation profile. At each update instance, the direction for the mathematical parallel model is obtained by the auto-differentiation with respect to the parallel model's parameters  $W_{\text{parallel}}$ . The physical control perturbation is determined by the AT estimator which defines how the parallel model update direction is mixed with a pseudo update direction from the BP of the physical error. The updates to the two systems are computed in parallel with the same set of parameters by concatenating the error matrices from the physical device and the parallel model, reducing the computational resources required to comparable level of a standard BP. (The update direction visualization is shown in three dimensions for easier viewing but should be  $N$  dimensions for  $N$  physically tunable parameters.)

With the AT method, the parallel model's parameter and the PNN's controls are initialized with the same set of randomized values. We know that the physical transformation of the PNN is different from the mathematical transformation of the parallel model even with the same set of parameters. We can now conceptualize two paths (Fig.1): one is the mathematical transformation of the parallel path, described as a simple mathematical differentiable model; the other is the physical path, described by only the hypothesized mapping for control parameters and the output prediction. For propagating the same piece of information through the two paths (where the physical input suffers from some inevitable inaccuracy), we obtain two predictions. The physical system's predictions become mathematically describable once the information is read out. We can thus measure the errors of these two predictions from the same target.

Given the two errors are computed as  $\mathbf{E}_{\text{photon}}$  and  $\mathbf{E}_{\text{parallel}}$ , we can auto-differentiate with respect to the mathematical parallel model's parameters,  $\mathbf{W}_{\text{parallel}}$  and  $\mathbf{b}_{\text{parallel}}$ . The two sets of errors would result in two sets of update directions for each controllable parameter. For the auto-differentiation of  $\mathbf{E}_{\text{parallel}}$ , the directions are directly associated with the gradient of the mathematical transformation as  $\Delta \mathbf{W}_{\text{parallel}} = \partial L / \partial \mathbf{W}_{\text{parallel}}$ .

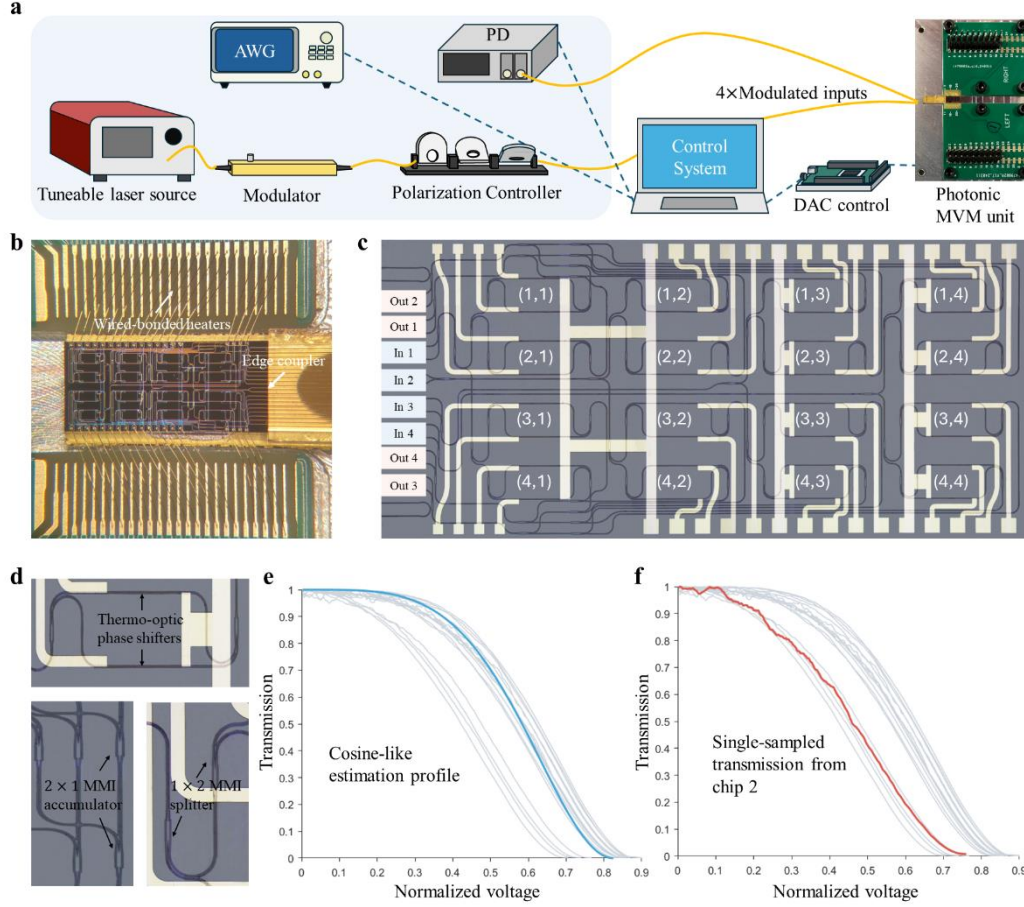


Fig.2 Implementation of a deep PNN with PIC. **a**, A schematic showing the setup for demonstrating a PNN with the SiN chip, where the yellow lines represent fibers for the optical path. **b**, Packaging for the photonic chip, including the wire-bonded heaters and edge coupled fiber array. **c**, The layout of the  $4 \times 4$  chip, indicating the connectivity of neurons enabled by the tuning of MZI units. **d**, Components representing the connectivity of neurons. The two-stage  $1 \times 2$  MMI splitters is the distribution of information from each neuron, and the two-stage  $2 \times 1$  MMI combiners represent the neuron accumulation. **e**, **f**, The two estimation profiles for controlling the physical parameters. The blue line represents the profile from the cosine-like function, and the red line is a single sampled profile from another copy of the chip.

In contrast, the directions from the auto-differentiation of  $E_{\text{photon}}$  carries no direct update indication for the physical control setting. We call the update directions obtained this way the pseudo directions,  $\Delta \mathbf{W}_{\text{pseudo}}^{[l]}$ . The dissociation between the physical transformation and the mathematical transformation of parameters  $\mathbf{W}_{\text{paral}}$  and  $\mathbf{b}_{\text{paral}}$  means the pseudo update is not useful on its own.

For regulated perturbation ( $\Delta \mathbf{W}_{\text{photonic}}^{[l]}$ ) to the physical parameters, we define the AT estimator as a mixture of the two update directions for each controllable parameter. The AT estimator is modulated by the mixing ratios  $M_{w1}$  and  $M_{w2}$ , representing the contributions of the two updates to the overall physical control update.

$$\Delta \mathbf{W}_{\text{photonic}}^{[l]} = M_{w1} \cdot \Delta \mathbf{W}_{\text{parallel}}^{[l]} + M_{w2} \cdot \Delta \mathbf{W}_{\text{pseudo}}^{[l]} \quad (3)$$

The typical values for  $M_{w1}$  and  $M_{w2}$  are 0.5. At each time step (defined by the update instance), the mathematical transformation of the parallel model is updated by the direction of  $\Delta \mathbf{W}_{\text{parallel}}^{[l]}$ , and the physical control parameter settings are perturbed by  $\Delta \mathbf{W}_{\text{photonic}}^{[l]}$ , both under the modulation of the same  $\alpha$  value. The updates at each time step are different for the mathematical transformation and physical controls, creating asymmetry in the settings, and thus

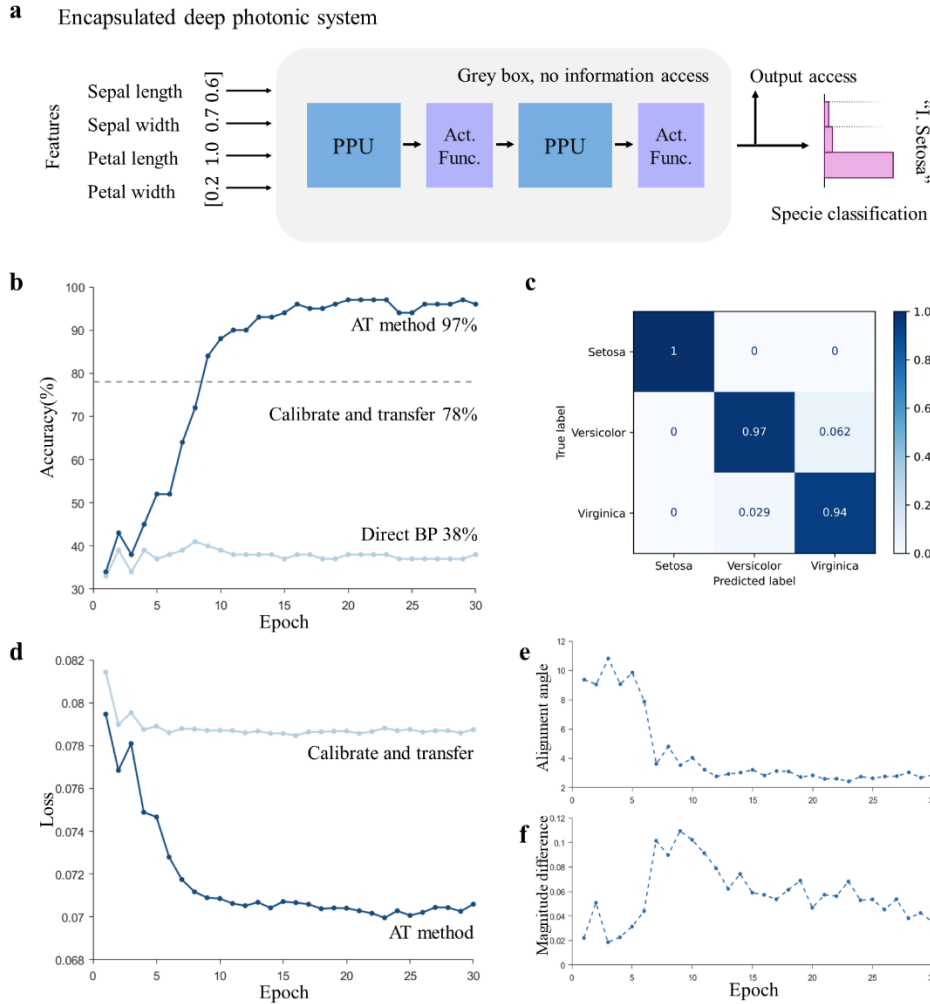


Fig.3 **a**, Schematic for an encapsulated deep PNN structure built from physical processing units (PPUs) of PICs. The access point to the physical network information is only at the output prediction. **b**, Accuracy for classifying the Iris species based on the four features. AT methods largely improved the accuracy from a standard BP of 38% to 97% for a grey box structure. The accuracy achieved is also higher than a system trained with BP based on partial information. **c**, Confusion matrix for the Iris dataset trained with the AT method. **d**, The AT method achieves a lower loss than a system which is trained with partial-information BP. **e, f**, The alignment angle and magnitude difference for the physical transformation from an idealistic transformation with the AT method. A reduction of alignment is not associated with the magnitude difference, showcasing the AT method's mechanism to train based on aligning the physical transformation towards the parallel model's transformation.

giving the name of this method. We can attribute AT's ability of training to concepts such as alignment<sup>19,20</sup>, and the PNN's inherent ability to cluster-and-separate<sup>12,13</sup> (a concept also seen for general NN structures of complexity via visualization techniques such as t-SNE<sup>36</sup>). More details on the concept of AT can be found in Methods and Supplementary S2.

## AT method for encapsulated grey-box physical NNs

Accompanying the previously mentioned common advantages of not enforcing the PNN to a mathematical representation, a fully encapsulated and packaged system also achieves the highest computational speed possible as only the physical information propagation time<sup>31</sup>. We demonstrate the AT method's ability to achieve performance

level near the theoretical maximum on a deep network structure of [4, 4, 3] (where each number represents the number of neurons in the layer) with PICs for classifying Iris flower species<sup>37</sup>.

The grey-box PNN is constructed with a  $4 \times 4$  SiN photonic chip as shown in Fig.2 (a). Details for the packaging, layout, and components of the PIC can be found in Fig.2 (b-d). The photonic neuron connection is enabled by a broadcast-select topology, which defines the topological neuron connectivity of the PNN. The  $1 \times 2$  multi-mode interferometers (MMIs) are responsible for distributing and accumulating the neuron information. The physical control parameters are the voltage applied to the thermos-optic phase shifters in a Mach-Zehnder interferometer (MZI) cell which adjusts the power transmission and thus the connection strength between neurons. The four input channels represent the four features of petal length, petal width, sepal length, and sepal width. The three neurons in the output layer represent the one-hot encoding for the three Iris species of Setosa, Versicolor, and Virginica.

As part of the procedure for conducting the AT method, we need to acquire an estimation profile mapping for the physical control parameters. Two approaches are used for acquiring statistically relatable profiles (Fig.2 e, f). The first approach is a quick theoretical estimation based on the components in the PIC PNN system. The physical control parameter (applied voltage) is associated with the physical transformation of the system via transmission of the MZI. A simple estimation of the control-transformation mapping is therefore through the stack of transfer matrices in each MZI element. An idealistic transmission can be described by a cosine-like function with respect to the power as follows. The transmission  $T$  is controlled by the applied voltage  $V$  under the modulation of some constant  $\gamma$ .

$$T = \frac{1}{2}(1 + \cos(2\gamma V^2)) \quad (4)$$

Alternatively, to showcase the AT method’s generalization for any sensible mapping profile estimation provided, we single-sampled a transmission profile from another copy of the SiN photonic chip. This sampled estimation profile is distorted by the errors in the physical computing system. The same estimation profile is applied to all physical controllable parameters for operating the grey-box PNN.

We first attempt to train the PNN with the BP update directions and the estimation profile as a reference. Foreseeably, the lack of accurate information for the control-transformation mapping reduces the accuracy of classification to 38%. With a three-class task of the Iris flower, this accuracy is close to a random guessing of 33%.

The PNN is then trained with the AT method as an update direction estimator, and the classification accuracy is vastly improved to 97% (for both estimation mapping profiles) (See Fig.3 (b) and Supplementary SFig.4). We benchmark the performance of the AT method with two approaches. The first is the BP accuracy achieved if some level of physical information is available via elementwise characterization (see supplementary S1). The second is the theoretical possible maximum accuracy of a model with perfect information under the same network structure.

A quick elementwise characterization of the MZI units is performed, and BP is used to train the PNN again. The resulting accuracy is 78% (indicated by the horizontal line of calibrate and transfer in Fig.3 (b)). The maximum possible accuracy with perfect information is 97% for this [4, 4, 3] structure. We see that the AT method achieves better performance for a grey-box PNN than BP, even when the BP updates have access to some level of knowledge of the system (Fig.3 (d)). The AT method performance is also close to the maximum benchmark for a system of perfect information.

We subsequently perform an analysis comparing the actual physical transformation of the PNN system and the idealistic transformation of the parallel model in Fig.3 (e, f). As the training progresses, the alignment angle (see Methods) is reduced, but the magnitude difference between the transformations ends at a higher level than their initial states. The disjoint between transformational angle separation and magnitude difference supports AT method’s theory to train based on the alignment of transformations.

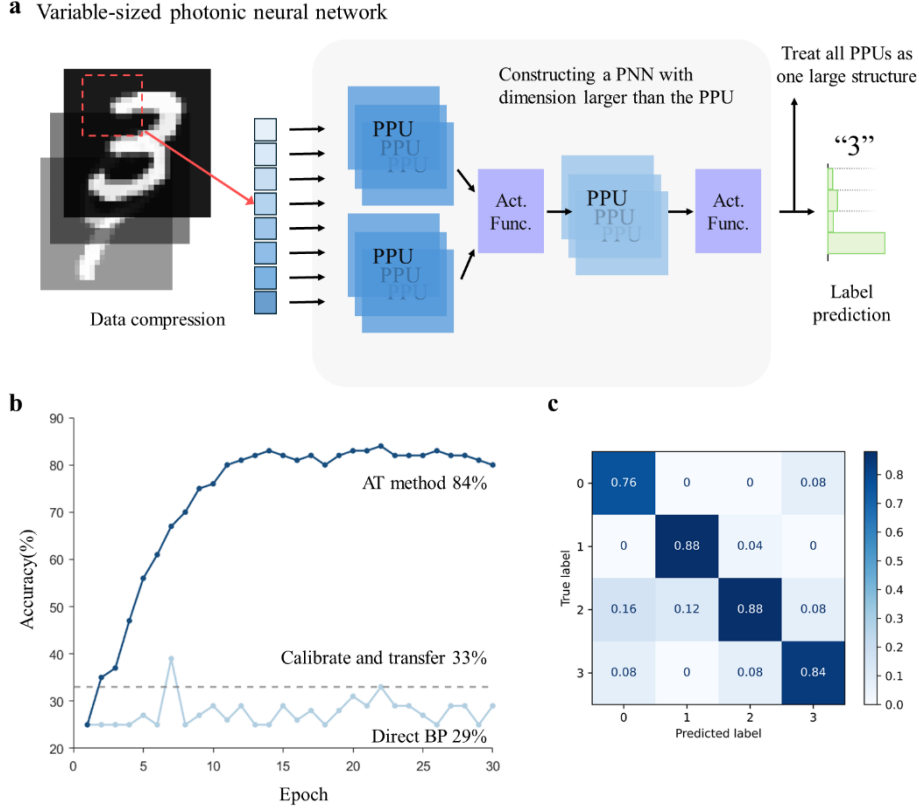


Fig.4 **a**, Schematic of a variable sized PNN constructed by stacking PPUs to achieve processing for sample dimensionality higher than the dimension of each PPU. **b**, The accuracy for identifying a modified MNIST hand-written classification task with the AT method improving the accuracy from 29% to 84%. The maximum possible accuracy for the equivalent network structure is 85%. The accuracy for direct BP and partial-information BP both drop to a low level due to the extensive accumulation of inaccuracy in knowledge. The AT method treats the overall structure as a larger PPU with the new sets of physical boundaries applied and is therefore not affected by the accumulation in knowledge inaccuracy. **c**, Confusion matrix for training the modified hand-written digit classification with the AT method.

## Scalability of the AT method for variable sized NN with stacked grey boxes

While a fully encapsulated PNN system offers the fastest computational speed possible, physical computation schemes often require some scaling techniques in spatial<sup>32</sup> and temporal<sup>38,39</sup> domains for general processing of information with a mismatched dimensionality to the physical hardware. Here we experimentally showcase the AT’s scalability for training scaled-up PNNs by stacking grey boxes of physical processing units (PPU) (see Fig.4 (a)).

We use a more complex image classification task with a modified MNIST hand-written digit dataset, utilizing a network structure of [8, 4, 4]. We use the same setup of the SiN chip, with the cosine-like function as the estimation profile for the physical control parameters. (See Methods for more details on the experiment.)

Similar to the previous demonstration, we start by attempting to train the combined PNN with BP given the estimation profile. The accuracy obtained from the training is 29%. For the four-class task presented here, the random guessing reference is 25%. We see a significant performance degradation with BP when the physical information is not available. When the AT estimator is used to train the PNN, the accuracy is enhanced to 84% (see Fig.4 (b)).

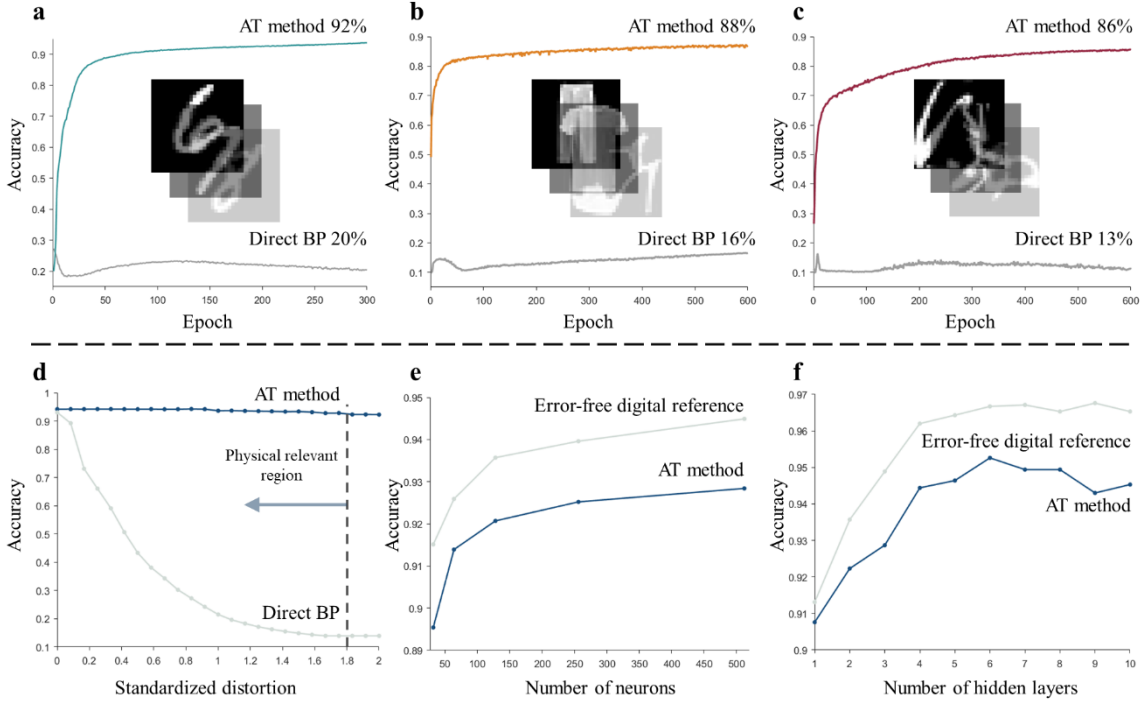


Fig.5 **a, b, c**, Training three datasets of MNIST, Fashion-MNIST, and Kuzushiji-MNIST with the AT method for PNNs. The training for all three datasets sees a large improvement in test accuracy. For benchmarking, the test accuracy achieved by an error-free model of the equivalent structure is 94%, 89%, and 88% for MNIST, F-MNIST, and K-MNIST, respectively. In all three cases, the AT method has managed to retrieve a level of performance close to the maximum possible for the network structure. **d**, Experimentally characterized variation is defined as one unit of standardized distortion of the physical transformation. An extended range of error analysis demonstrates AT method’s ability to maintain performance for all physically relevant region. **e, f**, Analysis for the AT method over different network structure including changing number of hidden layers and number of neurons in each hidden layer. AT method manages to retrieve similar performances to an error-free benchmark.

The two accuracy benchmarks of BP with limited information and theoretical maximum for this network structure are 33% and 85%, respectively. We see a retrieval of performance near the theoretical maximum with AT (84% from 85%). The performance degradation for calibrate-and-transfer partial-information BP is exacerbated compared to the previous demonstration (Fig.4 (b)). The accumulation of inaccuracies from each PPU results in an overall enlarged inaccuracy of information for the BP computation. On the other hand, the AT method treats the stacked grey-box PPUs as a larger sized grey-box PPU (regulated by the new physical boundary values) and is not affected by the imperfect information accumulation through repetitive use. (See details in Methods and Supplementary S1.)

## Generalization and repeatability of the AT method

We further demonstrate the repeatability of the AT method to retrieve near theoretical maximum performance for datasets of varying complexities and network structures through simulation. From the characterization of the photonic chip in the demonstration, we define maximal variation from a center value as an overestimation of one standardized distortion  $\sigma_{\text{photon}}$  of imperfect knowledge for the PPU. The random sources of errors are also considered for the simulation, we choose a noise floor of 10 dB signal-to-noise ratio, which is a higher noise level than most photonic computation systems would encounter (See Methods, Supplementary S2, and S3).

Three datasets of MNIST, fashion-MNIST (FMNIST), and Kuzushiji-MNIST (KMNIST) are used for the analysis. In all three cases, we observe improvements for training the grey-box PNN over the BP method (Fig.5 (a-c)). Specifically, the AT estimator achieves test accuracy of 92%, 88%, and 86% for the MNIST, FMNIST, and KMNIST,



respectively. In comparison, the test accuracy achieved by BP updates are 20%, 16%, and 13%. We benchmark the AT performance with the theoretical maximum based on perfect information PNNs. The theoretical maximum is 94%, 89%, and 88% for the three datasets, respectively. We see a consistent trend of retrieving performance comparable to the maximum with AT.

The AT method is analyzed through pressure test of varying distortion for the physical control-transformation mapping information (Fig.5 (d)). The test accuracy of the MNIST dataset is maintained over 90% for the all the range simulated from 0 to  $2 \sigma_{\text{photon}}$ . We also note that only the region below  $1.8 \sigma_{\text{photon}}$  is relevant to the physical boundary values (See Methods and Supplementary S1, S2). Consequently, for all the physically relevant regions, the AT method exhibits a well-behaved training to the performance levels comparable to the maximum. The network structure of the PNNs is varied for both the number of neurons in a hidden layer and the total number of hidden layers (Fig.5 (e, f)). For a variation of neuron numbers between 32 and 512, the accuracy difference for the MNIST dataset is maintained below 2% for AT on the physical NN from a maximum accuracy benchmark. The accuracy difference is maintained under 2.5% for changing the number of hidden layers from 1 to 10.

## Discussion

The AT method enables training a grey-box PNN with little known information. Here we discuss why treating the PNN as a grey box for training is desirable. When we enforce a mathematical representation onto the PNN system, we are requiring some type of feedback from the physical domain for each controlled physical parameter under perturbation. For a mathematical description of an DNN, access to the transformation information during the propagation is inherent. However, for any physical system, information access is never free.

Taking the implementation of PNN on PICs as an example, the access to information inside the hidden network structure (either for the detailed layer-wise calibration, or the in-situ computation of the physical gradient) would corresponds to some readout structure at each hidden layer. The additional readouts inside the deep PNN would mean a few things. To start with, additional hardware on-chip (such as a photodetector) adds to the footprint of the device and increases the cost for fabrication. In addition, the processing speed of an integrated photonic system is usually bottlenecked by the analogue-digital conversion stages. The reliance on the intermediate hidden information restricts the physical propagation speed during the training to those bottlenecks. Furthermore, the low propagation loss of photonic information implies very limited flavors of optical memories<sup>40</sup>. This means the access to photonic information requires power splitting. For maintaining the signal fidelity, amplification is required by using semiconductor optical amplifiers<sup>41</sup>. The inclusion of these active components not only adds to the cost via fabrication, but also increases the power consumption for operation. While the above discussion is for integrated photonic systems, many arguments hold true for other integrated PNNs such as analogue electronics based on resistive-switching materials<sup>7</sup> or phase change materials<sup>42</sup>. These factors combined could heavily undermine the advantages of implementing PNNs.

Many of the previous works<sup>28,43-47</sup> on training PNNs are still based on the concept of finding a sensible mathematical representation of the physical transformation, which inevitably leads to the need for accessing information in a deep neural network structure. Some previous methods which treats the PNN system as a grey box train at the cost of multiple propagations for the same piece of information through the physical structure<sup>48,49</sup>. The AT method aims at a balance, reducing the information required from the system to only the input, topological connectivity, and output prediction yet not increasing the number of propagations through the physical structure. The need for the input and output information in and out of a deep PNN structure cannot be avoided for any training method. The topological connectivity of neurons is also a known information for most scalable PNN implementations. The additional computation required for the AT method is a path in the parallel model. Nonetheless, this is a smaller overhead compared to the extra hardware overheads for many of the methods mentioned. In addition, the computation of the AT update estimator is based solely on the parallel model's parameters, meaning the update to both paths can be done in parallel by concatenating the error matrices from the physical and mathematical transformations. The required computational resource for the AT estimator is therefore very similar to a standard BP gradient computation. Overall, the AT method serves as a robust light-weight alternative to training deep PNNs with little information, requiring the minimal hardware (same as the inference stage), and reduced computational overhead (comparable to a standard BP).

## Conclusion

In this paper, we present the asymmetrical training method as an alternative update direction estimator for PNNs. The AT method treats the PNN as a grey box structure, requiring little information about the physical system. When provided with only the input, output, and neuron topological connectivity, we showcased the AT method’s enhanced performance over BP across tasks including the Iris flower, MNIST, FMNIST, and KMNIST. The features of the AT method indicate its suitability as a light-weight alternative training method for integrated PNN systems where the cost for accessing information within the structure is high. Most PNN systems are designed as a co-standing part with some digital assistant system for blending into the modern technology ecosystem. The reduced hardware and computational overhead from the AT method could potentially help PNN devices to be implemented in a wider range of applicational scenario, and potentially near the points of data generation for NN computation at a reduced cost.

## Methods

### Asymmetrical training estimator

The AT method can be best understood from the concept of the alignment. We invoke the expression for a general alignment angle between two transformations  $\mathbf{A}$  and  $\mathbf{B}$  as the angle  $\beta$ . The training behavior of the alignment-based training is heavily inspired by the parallel information propagation for neurons in a biological system. The details and formalism of the training with alignments are not repeated here, but can be found in reference<sup>19,20</sup>. The concept of alignment training states that the updates work towards the reduction of loss if the alignment between the update  $\Delta\mathbf{W}$  and the gradient  $\delta\mathbf{W}$  are within the alignment of  $90^\circ$ .

$$\cos(\beta) = \frac{\mathbf{B}^T \mathbf{A}}{\|\mathbf{B}^T\| \|\mathbf{A}\|} \quad (5)$$

While simply invoking the alignment training concept, we think about what the physical transformation in a deep PNN system is. We start with the discussion by considering a classical system, where finite feedback from a finite perturbation applies for all the physical parameters’ transformations. For each given perturbate-able control parameter, the deviation for the idealistic control  $W_{\text{photon}}$  and the resulting transformation  $T_{\text{photon}}$  can be described by some physical functional distortion of  $F_{\text{photon}}(\cdot)$ . We note that the same concept can be applied to the mathematical transformation, but the function of  $F_{\text{paral}}(\cdot)$  is unity, and we obtain  $T_{\text{paral}} \equiv W_{\text{paral}}$ .

We know the description of a loss function is a functional surface of  $N$ -dimension for a total  $N$  number of controllable parameters measuring the separation between prediction and target. Regardless of a discrete or continuously encoded physical system, we can think about the position of the physical transformation in a general loss-function space of  $2N$  dimensions as a tensor for different levels of distortions in the parameter pair of  $(W_{\text{photon}}, T_{\text{photon}})$ . We can conceptualize the variation of the distortion level as frontiers of the loss-function surfaces stacked with each other by the quantized minimal step (easiest to visualize if only think about the change in one parameter at a given time). Equally, we also know that the functional deviation of the parallel model pair of  $F_{\text{paral}}(\cdot)$  is describable by some very specific pair of physical parameters (corresponding to the case with perfect information). Therefore, we understand that there must be some sensible perturbations to the physical controls which moves the loss-function description of the PNN towards the loss-function description of the mathematical parallel model.

Nonetheless, finding this exact perturbation direction inevitably associates with the extraction of information in the hidden layer of the PNN system. We don’t want intermediate information extraction for the grey-box training of our AT method. Consequently, we need a relaxation from that exact perturbation and define alignment criteria as is the case seen in the alignment-based training methods. The robustness of the AT method originates from its root in the gradient-based update for the parallel model. We know that for any sensible network structure, the gradient-based update leads to a minimum (local or global) in the loss function. Consequently, a well-behaved training for AT is logically associated with the regulation towards the gradient update of the parallel model. The first criterion is therefore for the alignment between the AT estimator update direction  $\Delta\mathbf{W}_{\text{AT}}$  and the parallel model gradient  $\delta\mathbf{W}_{\text{paral}}$ . This criterion is similar to the concept of direct feedback alignment<sup>20</sup>. Nevertheless, we can recognize that this criterion on its own is not capable training the PNN, because the accumulated action in the loss-function surface of the parallel model is projected to a different loss value for the loss-function surface of the physical structure.

Consequently, we require a second criterion for successful training. At each time step of update instance, for a small modulation of the perturbation ( $\alpha \ll ||\mathbf{W}||$ ), the deviation between the control and transformation can be described by a first-order approximation as a projection of  $\mathbf{T} = \mathbf{D}^t \mathbf{W}$  for  $t = t'$ . We are thus requiring the AT estimator's update aligning towards the transpose of that projection  $(\mathbf{D}^t)^T$ . We notice the importance of avoiding the projection accumulation through the separated layers of the network with the regulation of the parallel model's propagation information  $\mathbf{z}_{\text{para}}$  and  $\mathbf{a}_{\text{para}}$ . Therefore, with all these conditions combined, we can logically derive the form of the AT estimator direction as the mixture of the auto-differentiated physical error and mathematical error with respect to the parallel model's parameters, as highlighted by Eq. (3).

We can thus see the origin of the equally distributed mixing ratio of  $M_{w1}$  and  $M_{w2}$  for the modulation of the pseudo and parallel update directions as they converge to similar magnitudes for successful training. We see the success of alignment for all physically relevant regions. The alignment criteria could be satisfied given the initial transformation alignment is within  $90^\circ$ . We highlight the importance of a physically encoded system for the AT method (See details in Supplementary S2). One of the differences between a physical transformation and an arbitrary mathematical transformation is the physics-defined boundary conditions. The physical boundaries govern the representable range of the physical transformation. This means that given the physical device is functional, the breakage of the alignment condition is statistically rare (See Supplementary S2). If we consider the deviation as described by the standard normal distribution. For a deviation of ten percent of the physical boundary range, the probability of breaking the alignment is  $1.5 \times 10^{-21}\%$ , even for an extreme deviation of half the physically representable range, the probability of breaking the alignment is only 2.5% (See Supplementary S2). Consequently, the characteristics of a PNN system help preserve the robustness and aid successful training with the AT method.

### Grey-box AT for calibration-free training on PIC NNs

We can notice the ability of the AT method to train PNN as grey box is also reflected as the simplicity to operate the PNN system without any need for a pre-training calibration. The construction of the PNN is based on the  $4 \times 4$  and  $4 \times 3$  neuron connections enabled by the SiN PIC device for the Iris task. The neuron connectivity for the modified MNIST is  $8 \times 4$  and  $4 \times 4$ . The  $8 \times 4$  connectivity is of higher dimension than the PPU, which requires the further decomposition into two copies of PPUs with connectivity of  $4 \times 4$ .

The characterization of the SiN chip is performed with a 16-bit DAC and a driver circuit for a voltage application to each heater in the MZI between 0 and 32V. We limit the quantized modulation of both the variable optical attenuator and the MZI units to only 100 levels. The defined quantization is associated with the requirement for a modest extinction ratio of -20dB. Non-linearity is applied to the signal propagation digitally. However, the profiles of the non-linearity is defined by the photonic structures of micro-ring resonators demonstrated by previous literature<sup>31,43,50</sup>. For each instance that the photonic chip is used to represent part of the neuron connection, we add an additional shift to estimation profile for representing the varying behavior of the separated parts in a physical NN. With the prediction from the physical and mathematical models, the classification is performed based on an argmax function.

The key to successful training with the AT method involves the correct definition of the relevant physical boundaries for the parallel model. For example, with the PIC implemented PNN, we know the physical transformation on the propagated information is contained within the range of minimum and maximum optical power. Therefore, the construction of the parallel model should also have transformation described by the same representable range. While the definition is for each element, we know the system level distortion can be attributed back towards the individual elements. The appropriate boundary definitions allow the correct understanding of the maximum possible neuron activation level for reference. The reference of physically representable maximum neuron activation also allows the proper modification of the physical nonlinearity. (See Supplementary S1, and Supplementary figures SFig.1-6 for more details on the experiment.)

The dataset used for the Iris flower classification is based on the original dataset<sup>37</sup>. The MNIST dataset is modified to be suitable for demonstration on the PIC-based PNN. The original  $28 \times 28$  pixel image which flattens to 784 features contain largely zeros and is compressed to 8 features through principal component analysis<sup>31</sup>. The input dimensionality is still larger than the PIC size, which requires the decomposition of the  $8 \times 4$  neuron connections to two temporal copies of  $4 \times 4$  connections for accumulation. For the modest network structure of [8, 8, 4], the original ten-class task

is thus reduced to a four-class task of digits 0, 1, 2, and 3, matching the number of ports on the photonic chip for one-hot encoding.

### Simulation of physical NN training with AT method

As defined in previous discussions, we can think about the contribution to the overall transformation as the distortion with respect to the control of the physical parameters. We also note that the system-level information distortion can be mathematically distributed back at each tunable parameter given that the topological neuron connectivity of the system is static. Apart from the distortion of the control mapping information, we also add physical errors such as noise and random fluctuations to the model. For achieving reliable results, we use the worst-case overestimation wherever possible in the simulation. A description for simulating the distortion to each physical parameter’s transformation is given as follows.

$$F_{\text{photon}}(W_{\text{photon}}) = (I + P) \otimes (W_{\text{photon}} + N_{\text{init}}) + N_{\text{rand}} \quad (6)$$

The distortion at each time step is defined by  $P$ , where the  $\otimes$  denotes the element wise Hadamard product for linear overestimation of the deviation across tunable range. The parameter is subject to some fixed initial random distortion of  $N_{\text{init}}$ . At each instance the information is passed through the physical structure, a randomized error  $N_{\text{rand}}$  is added to represent the signal degradation. For characterizing a standardized deviation, the experimentally determined variation of the MZI unit is used for reference. As seen in the characterized profiles in Fig.2 (e, f). Half the maximal variation between the leftmost and rightmost profile is used as one standard deviation for generating the distortion for each element, corresponding to a value encoding variation of  $\pm 60\%$  with  $1 \sigma_{\text{photon}}$ . The chosen encoding value-based distortion allows both the overestimation of the transmission error and generalization to other PNN systems.

We apply the AT method on three different image classification datasets, for classifying hand-written digits (MNIST), Kuzushiji characters (KMNIST), and fashion items (FMNIST). We choose one-hot encoding for the labels in all three cases. Each sample image has an original  $28 \times 28$  pixels resolution, which is flattened to 784 input features. The network structures for the three tasks are  $[784,128,128,10]$ ,  $[784,256,256,10]$ , and  $[784,256,256,10]$  for MNIST, FMNIST, and KMNIST, respectively. The hidden layers are connected by ReLU activation functions emulating on-chip MRR nonlinearities<sup>31</sup>, while the output activation is a SoftMax layer. The learning rate is varied depending on the task, but within a general range of  $3 \times 10^{-5}$  to  $1 \times 10^{-4}$ . We use a simple gradient descent optimizer for our simulations, alternative optimizer can also be used in conjunction with the AT estimator. We use a batch size of 600 for training. At each epoch, the data is shuffled to avoid memorization of the dataset. The standard MNIST dataset is trained for 300 epochs, the FMNIST and KMNIST are both trained for 600 epochs. All the simulations are written with Python predominantly using Numpy<sup>52</sup>, Tensorflow<sup>53</sup>, Sklearn<sup>54</sup>, and Pytorch<sup>55</sup> packages.

## Acknowledgement

This work was supported by the European Union’s Horizon 2020 research and innovation programme, project INSPIRE, and UK EPSRC, project QUDOS (EP/T028475/1).

## Code availability

The code used in this study is available from the corresponding author upon request.

## Data availability

Data related to this publication is available from ...

## Author contribution

Y.W. conceptualized the idea, demonstrated the experiments, and performed the simulation. M.C. helped with the experiments. C.Y. designed the photonic chip layout. M.C., J.M. and T.Y. helped with the packaging of the photonic chip. Q.C. and R.P. supervised the project. Y.W. and Q.C. prepared the manuscript. M.C. and C.Y. assisted with the preparation of the manuscript.

## Competing interest

The authors declare no competing interest.

## Reference:

1. LeCun, Y., Bengio, Y. & Hinton, G. Deep learning. *Nature* **521**, 436–444 (2015).
2. Alzubaidi, L. *et al.* Review of deep learning: concepts, CNN architectures, challenges, applications, future directions. *J Big Data* **8**, 53 (2021).
3. Sarker, I. H. Deep Learning: A Comprehensive Overview on Techniques, Taxonomy, Applications and Research Directions. *SN COMPUT. SCI.* **2**, 420 (2021).
4. Pandey, M. *et al.* The transformational role of GPU computing and deep learning in drug discovery. *Nat Mach Intell* **4**, 211–221 (2022).
5. Jouppi, N. P. *et al.* In-Datacenter Performance Analysis of a Tensor Processing Unit™.
6. Ielmini, D. Brain-inspired computing with resistive switching memory (RRAM): Devices, synapses and neural networks. *Microelectronic Engineering* **190**, 44–53 (2018).
7. Zahoor, F., Azni Zulkifli, T. Z. & Khanday, F. A. Resistive Random Access Memory (RRAM): an Overview of Materials, Switching Mechanism, Performance, Multilevel Cell (mlc) Storage, Modeling, and Applications. *Nanoscale Res Lett* **15**, 90 (2020).
8. Reuther, A. *et al.* Survey of Machine Learning Accelerators. in *2020 IEEE High Performance Extreme Computing Conference (HPEC)* 1–12 (2020). doi:10.1109/HPEC43674.2020.9286149.
9. Bavikadi, S. *et al.* A Survey on Machine Learning Accelerators and Evolutionary Hardware Platforms. *IEEE Des. Test* **39**, 91–116 (2022).
10. Whittington, J. C. R. & Bogacz, R. Theories of Error Back-Propagation in the Brain. *Trends in Cognitive Sciences* **23**, 235–250 (2019).

11. Lillicrap, T. P., Santoro, A., Marris, L., Akerman, C. J. & Hinton, G. Backpropagation and the brain. *Nat Rev Neurosci* **21**, 335–346 (2020).
12. Vandoorne, K. *et al.* Experimental demonstration of reservoir computing on a silicon photonics chip. *Nat Commun* **5**, 3541 (2014).
13. Gauthier, D. J., Boltt, E., Griffith, A. & Barbosa, W. A. S. Next generation reservoir computing. *Nat Commun* **12**, 5564 (2021).
14. McMahon, P. L. *et al.* A fully programmable 100-spin coherent Ising machine with all-to-all connections. *Science* **354**, 614–617 (2016).
15. Cen, Q. *et al.* Large-scale coherent Ising machine based on optoelectronic parametric oscillator. *Light Sci Appl* **11**, 333 (2022).
16. Amari, S. Backpropagation and stochastic gradient descent method. *Neurocomputing* **5**, 185–196 (1993).
17. Ruder, S. An overview of gradient descent optimization algorithms. Preprint at <http://arxiv.org/abs/1609.04747> (2017).
18. Kingma, D. P. & Ba, J. Adam: A Method for Stochastic Optimization. Preprint at <http://arxiv.org/abs/1412.6980> (2017).
19. Lillicrap, T. P., Cownden, D., Tweed, D. B. & Akerman, C. J. Random synaptic feedback weights support error backpropagation for deep learning. *Nat Commun* **7**, 13276 (2016).
20. Nøkland, A. Direct Feedback Alignment Provides Learning in Deep Neural Networks. Preprint at <http://arxiv.org/abs/1609.01596> (2016).
21. McMahon, P. L. The physics of optical computing. *Nat Rev Phys* **5**, 717–734 (2023).
22. Feldmann, J. *et al.* Parallel convolutional processing using an integrated photonic tensor core. *Nature* **589**, 52–58 (2021).

23. Zhou, H. *et al.* Photonic matrix multiplication lights up photonic accelerator and beyond. *Light Sci Appl* **11**, 30 (2022).
24. Minzioni, P. *et al.* Roadmap on all-optical processing. *J. Opt.* **21**, 063001 (2019).
25. Tian, Y. *et al.* Scalable and compact photonic neural chip with low learning-capability-loss. *Nanophotonics* **11**, 329–344 (2022).
26. Bernstein, L. *et al.* Freely scalable and reconfigurable optical hardware for deep learning. *Sci Rep* **11**, 3144 (2021).
27. Lin, X. *et al.* All-optical machine learning using diffractive deep neural networks. (2018).
28. Zhou, T. *et al.* Large-scale neuromorphic optoelectronic computing with a reconfigurable diffractive processing unit. *Nat. Photonics* **15**, 367–373 (2021).
29. Wang, J., Sciarrino, F., Laing, A. & Thompson, M. G. Integrated photonic quantum technologies. *Nat. Photonics* **14**, 273–284 (2020).
30. Pelucchi, E. *et al.* The potential and global outlook of integrated photonics for quantum technologies. *Nat Rev Phys* **4**, 194–208 (2021).
31. Ashtiani, F., Geers, A. J. & Aflatouni, F. An on-chip photonic deep neural network for image classification. *Nature* **606**, 501–506 (2022).
32. Xu, Z. *et al.* Large-scale photonic chiplet Taichi empowers 160-TOPS/W artificial general intelligence - Supplementary Material. *Science* **384**, 202–209 (2024).
33. Li Deng. The MNIST Database of Handwritten Digit Images for Machine Learning Research [Best of the Web]. *IEEE Signal Process. Mag.* **29**, 141–142 (2012).
34. Xiao, H., Rasul, K. & Vollgraf, R. Fashion-MNIST: a Novel Image Dataset for Benchmarking Machine Learning Algorithms. Preprint at <http://arxiv.org/abs/1708.07747> (2017).
35. Clanuwat, T. *et al.* Deep Learning for Classical Japanese Literature. Preprint at <https://doi.org/10.20676/00000341> (2018).

36. van der Maaten, L. & Hinton, G. Visualizing Data using t-SNE. *Journal of Machine Learning Research* **9**, 2579–2605 (2008).
37. Fisher, R. A. THE USE OF MULTIPLE MEASUREMENTS IN TAXONOMIC PROBLEMS. *Annals of Eugenics* **7**, 179–188 (1936).
38. Chen, M., Cheng, Q., Ayata, M., Holm, M. & Penty, R. An Iterative Photonic Processor for Fast Complex-valued Matrix Inversion. *Photon. Res.* (2022) doi:10.1364/PRJ.468097.
39. Zhang, H. *et al.* An optical neural chip for implementing complex-valued neural network. *Nat Commun* **12**, 457 (2021).
40. Alexoudi, T., Kanellos, G. T. & Pleros, N. Optical RAM and integrated optical memories: a survey. *Light Sci Appl* **9**, 91 (2020).
41. Tang, H. *et al.* A Review of High-Power Semiconductor Optical Amplifiers in the 1550 nm Band. *Sensors* **23**, 7326 (2023).
42. Wang, X., Li, W., Luo, Z., Wang, K. & Shah, S. P. A critical review on phase change materials (PCM) for sustainable and energy efficient building: Design, characteristic, performance and application. *Energy and Buildings* **260**, 111923 (2022).
43. Bandyopadhyay, S. *et al.* Single chip photonic deep neural network with accelerated training. Preprint at <http://arxiv.org/abs/2208.01623> (2022).
44. Pai, S. *et al.* Experimentally realized in situ backpropagation for deep learning in photonic neural networks. *Science* **380**, 398–404 (2023).
45. Wright, L. G. *et al.* Deep physical neural networks trained with backpropagation. *Nature* **601**, 549–555 (2022).
46. Hughes, T. W., Minkov, M., Shi, Y. & Fan, S. Training of photonic neural networks through in situ backpropagation and gradient measurement. *Optica* **5**, 864 (2018).



47. Zheng, Z. *et al.* Dual adaptive training of photonic neural networks. *Nat Mach Intell* (2023)  
doi:10.1038/s42256-023-00723-4.
48. Zhang, T. *et al.* Efficient training and design of photonic neural network through neuroevolution. *Opt. Express* **27**, 37150 (2019).
49. Momeni, A., Rahmani, B., Malléjac, M., Del Hougne, P. & Fleury, R. Backpropagation-free training of deep physical neural networks. *Science* **382**, 1297–1303 (2023).
50. Yu, W., Zheng, S., Zhao, Z., Wang, B. & Zhang, W. Reconfigurable Low-Threshold All-Optical Nonlinear Activation Functions Based on an Add-Drop Silicon Microring Resonator. *IEEE Photonics J.* **14**, 1–7 (2022).
51. Greenacre, M. *et al.* Principal component analysis. *Nat Rev Methods Primers* **2**, 100 (2022).
52. Harris, C. R. *et al.* Array programming with NumPy. *Nature* **585**, 357–362 (2020).
53. Abadi, M. *et al.* TensorFlow: Large-Scale Machine Learning on Heterogeneous Distributed Systems. (2015).
54. Pedregosa, F. *et al.* Scikit-learn: Machine Learning in Python. *MACHINE LEARNING IN PYTHON* (2011).
55. Paszke, A. *et al.* PyTorch: An Imperative Style, High-Performance Deep Learning Library. Preprint at <http://arxiv.org/abs/1912.01703> (2019).